

1997

## Variability in Forest Floor Mass and Nutrient Concentration of Mature Pine-Hardwoods in the Ouachita Mountains

Hal O. Liechty

*University of Arkansas at Monticello*


Michael G. Shelton

*USDA Forest Service*

Edwin R. Lawson

*University of Arkansas at Monticello*

Follow this and additional works at: <http://scholarworks.uark.edu/jaas>

 Part of the [Forest Biology Commons](#), and the [Forest Management Commons](#)

---

### Recommended Citation

Liechty, Hal O.; Shelton, Michael G.; and Lawson, Edwin R. (1997) "Variability in Forest Floor Mass and Nutrient Concentration of Mature Pine-Hardwoods in the Ouachita Mountains," *Journal of the Arkansas Academy of Science*: Vol. 51 , Article 18.

Available at: <http://scholarworks.uark.edu/jaas/vol51/iss1/18>

This article is available for use under the Creative Commons license: Attribution-NoDerivatives 4.0 International (CC BY-ND 4.0). Users are able to read, download, copy, print, distribute, search, link to the full texts of these articles, or use them for any other lawful purpose, without asking prior permission from the publisher or the author.

This Article is brought to you for free and open access by ScholarWorks@UARK. It has been accepted for inclusion in Journal of the Arkansas Academy of Science by an authorized editor of ScholarWorks@UARK. For more information, please contact [scholar@uark.edu](mailto:scholar@uark.edu).

# Variability in Forest Floor Mass and Nutrient Concentration of Mature Pine-Hardwoods in the Ouachita Mountains

Hal O. Liechty<sup>1</sup>

School of Forest Resources  
University of Arkansas, Monticello  
Monticello, AR 71656

Michael G. Shelton

USDA Forest Service  
Southern Research Station  
Monticello, AR 71656

Edwin R. Lawson

School of Forest Resources  
University of Arkansas, Monticello  
Monticello, AR 71656

<sup>1</sup>Corresponding author

## Abstract

Prior to timber harvesting, forest floor mass and nutrient concentrations in forest floor and mineral soil were determined in 24 mature, shortleaf pine (*Pinus echinata* Mill.)-hardwood stands occurring within the northern, eastern, southern and western sub-ecoregions of the Ouachita Mountains. The forest floor samples were collected at each of three locations representing the lower, mid, and upper slope positions within each stand. Samples of the L-(litter) and F-layers (fermentation) were collected separately. Materials from the L-layer were differentiated into hardwood foliage, pine foliage, and woody/reproductive components. Mass and nutrient concentrations of the various forest floor components were compared among slope positions and among sub-ecoregions to evaluate the influence of these factors on forest floor pools. Forest floor mass and nutrient concentrations generally did not differ among slope positions. Although mass did not differ among sub-ecoregions, forest floor concentrations of Ca, Mg, and Mn were significantly higher in the northern than the eastern or southern portion of the Ouachita Mountains.

## Introduction

The forest floor consists of organic matter on mineral soil surface which accumulates from forest aboveground biomass. This organic material is an important source of mineralizable nutrients/carbon and is an essential component of forest ecosystem energy/nutrient cycles. Spatial variation of forest floor characteristics within forest stands or among stands across the landscape can generally be related to the variation in abiotic or biotic factors. Soil parent material and climate are two abiotic factors which have been found to affect forest floor characteristics and are known to vary among slope positions and sub-ecoregions in the Ouachita Mountains (Graney, 1992; Baker, 1994). As part of a project addressing the effects of diversified harvesting and silvicultural treatments on various commodity and noncommodity resources in shortleaf pine (*Pinus echinata* Mill.) hardwood stands, we quantified the amount and chemistry of forest floor within 24 shortleaf pine-hardwood stands prior to harvesting in the Ouachita/Ozark National Forests. This information was used to determine if these forest floor characteristics differed among slope positions and sub-ecoregions in the Ouachita Mountains.

## Materials and Methods

**Study Area and Sampling Design.**--Twenty four relatively undisturbed, mature, shortleaf pine hardwood stands occurring in the Ouachita Mountains of Arkansas and

Oklahoma were included in this study. Only stands with the following attributes were considered for inclusion in the study: 1) average tree age >70 years, 2) stand area >14 ha, 3) stands on southern facing slopes, 4) pine basal area between 13.8 and 25.2 m<sup>2</sup> ha<sup>-1</sup>, and 5) hardwood basal area between 4.6 and 11.5 m<sup>2</sup> ha<sup>-1</sup>. From this general population of stands, six were randomly selected from within each of four sub-ecoregions representing the northern, western, eastern and southern portions of the Ouachita Mountains. These sub-ecoregions represent the general variation in land forms, soil, geology, and climate within this area (Clingenpeel and Cochran, 1992; Baker, 1994).

Each stand was subdivided into quarters to facilitate establishing 12 randomly located, permanent subplots that were used for sampling vegetation by other project components. These quarters were oriented perpendicular to the dominant slope within the stand. From a randomly chosen quarter within each stand the subplot representing the lower, middle, or upper portion of the slope was chosen for forest floor sampling (Shelton and Lawson 1994). In total, 72 subplots were sampled in the 24 stands.

**Field Sampling.**--Sampling was conducted during February and March of 1993. Five sampling locations were systematically located 11.4 m from each subplot center. Sampling locations were relocated if abnormal conditions such as large surface rocks, woody debris more than 7.5 cm in diameter, or previous manmade disturbance (e.g., old roads, etc.) occurred at the sampling location. Thus samples and results reflect potential optimal forest floor conditions from undisturbed areas which are not dominated by rocks

## Variability in Forest Floor Mass and Nutrient Concentration of Mature Pine-Hardwoods in the Ouachita Mountains

or woody materials rather than an average surface conditions in the stands as a whole. Approximately less than 5% of the sample locations had to be relocated due to these criteria. The forest floor was collected from within a 0.1-m<sup>2</sup> square frame at each sampling location. Two forest floor layers representing two stages of decomposition were collected. The first was a litter (L) layer, which included the uppermost, current year undecomposed plant material and the other a fermentation (F) layer consisting of partially decomposed/fragmented older material located above the mineral soil surface and below the L layer. The L and F layers are also commonly referred to as Oi and Oe horizons, respectively (Pritchett 1987). The humus layer, a thin layer of amorphous organic matter (Oa horizon) lying on top of the mineral soil, was not collected nor included with the F layer.

**Laboratory Procedures.**—Forest floor samples were dried at 75° C until a constant moisture content was obtained and then mass determined. Each L-layer sample was separated into woody and foliar components. The woody component included branches, bark, small stems, and reproductive material (e.g., pine cones). The foliar component of the samples for each subplot was separated into pine and hardwood foliage and weighed. Thus, the L-layer was represented by pine foliage, hardwood foliage, and woody components. All mass were expressed as totals and not corrected for loss on ignition as reported by Shelton and Lawson (1994).

Forest floor components were composited for a subplot and mass was determined. Then samples were ground to pass a 20-mesh sieve. Concentrations of P, K, Ca, Mg, Mn, Na, Cu, Fe, and Zn were determined by inductance coupled plasma (ICP) analysis after nitric/perchloric digestion (University of Arkansas, Soil Test Laboratory, 1990a). Total N concentrations were also determined using a Tecator Kjeltex Model 1030 Auto Analyzer after sulfuric acid/hydrogen peroxide digestion (University of Arkansas, Soil Test Laboratory, 1990b).

**Data Analysis.**—Forest floor data were analyzed using analysis of variance for a two factorial design. Sub-ecoregion and topographic position were the two factors. Mean separation was accomplished using Tukey's Honestly Significant Difference multiple-range test (Steel and Torrie 1980) at the  $\alpha=0.05$  after analysis of variance tests indicated differences in a factor were significant.

## Results And Discussion

**Slope.**—Comparison of forest floor nutrient concentrations and mass showed generally no significant or consistent differences among slope positions. Total L-layer (Table 1) macronutrient concentrations were very similar among the lower, mid, and upper positions. Concentrations for some micronutrients were higher in the lower slopes while concentrations of others such as Cu or Zn were higher in the

upper slopes. Regardless of the nutrient considered, differences among slope positions for any component in the L-layer were not significant.

Table 1. Forest floor total L-layer nutrient concentrations and mass by slope position.

	Lower	Mid	Upper
	----- % -----		
N	0.69	0.69	0.67
P	0.05	0.05	0.05
K	0.07	0.07	0.07
Ca	1.09	1.02	0.96
Mg	0.12	0.11	0.11
	----- mg kg <sup>-1</sup> -----		
Cu	10	12	15
Fe	326	229	227
Mn	1156	1056	968
Na	225	238	236
Zn	100	129	133
	----- 10 <sup>3</sup> kg ha <sup>-1</sup> -----		
Mass	5.6	5.1	5.5

Nutrient concentration and mass of the F-layer were also similar among slope positions. Only Zn had significantly different concentrations among the slope positions. Mean concentrations of Zn in the mid-slope position was (89 mg kg<sup>-1</sup>) and was significantly greater than concentrations in the upper slope position (89 mg kg<sup>-1</sup>). The general lack of differences in forest floor chemistry and mass among slope positions can be attributed to the high variation in slopes among stands and the methodology used to delineate slope position within a stand. Average slopes for the subplots ranged from 2 to 44% in the stands. Differences in forest floor concentrations or mass would likely be greater within stands which had greater slopes than stands with less slope. A number of stands occurred on landforms with minimal slopes and thus differences in forest floor among slope positions were minor as well.

Slope position of a subplot was delineated relative to the position of the subplot in the stand rather than its position along a landform. Designation of a subplot's slope position using the general landform rather than its location within the stand indicated that entire stands could occupy only one slope position. Given this lack of difference among slope positions, it was not surprising that differences in forest floor among subplots were inconsequential.

## Hal O. Liechty, Michael G. Shelton, and Edwin R. Lawson

**Sub-Ecoregion.**—Variability in nutrient concentrations among sub-ecoregions was greater than the variability among slope positions. Concentrations of Ca and Mg in the L-layer and Ca in the F-layer were consistently lower in the east region than in the north (Table 2) while Mn concentrations for all forest floor components were significantly lower in the southern region than the north (Table 3). Concentrations of Ca and Mg were 18-42% higher in the northern compared to eastern sub-ecoregion while concentrations of Mn was 30-33% higher in the northern compared to southern sub-ecoregion. All other nutrients, except Cu in the F-layer, did not significantly differ among sub-ecoregions.

Table 2. Macronutrient concentrations and mass of pine and hardwood (Hwd) foliage in the L-layer and in the F-layer (F) by sub-ecoregions.

		North	East	South	West
		----- % -----			
<b>N</b>	Pine	0.64a	0.68a	0.65a	0.66a
	Hwd	0.91a	0.90a	0.91a	0.94a
	F	0.94a	0.99a	1.02a	0.95a
<b>P</b>	Pine	0.05a	0.05a	0.05a	0.05a
	Hwd	0.06a	0.05a	0.05a	0.07a
	F	0.06a	0.06a	0.06a	0.06a
<b>K</b>	Pine	0.08a	0.07a	0.08a	0.07a
	Hwd	0.09a	0.08a	0.09a	0.10a
	F	0.11a	0.10a	0.09a	0.09a
<b>Ca</b>	Pine	0.66a	0.53b	0.62a	0.60ab
	Hwd	1.66a	1.30b	1.49ab	1.66a
	F	0.87a	0.62b	0.76ab	0.76ab
<b>Mg</b>	Pine	0.13a	0.11b	0.12ab	0.11b
	Hwd	0.20a	0.14b	0.17ab	0.17ab
	F	0.11a	0.11a	0.09a	0.10a
		----- 10 <sup>3</sup> kg ha <sup>-1</sup> -----			
<b>Mass</b>	Pine	1.72a	1.73a	1.73a	2.02a
	Hwd	1.68a	1.54a	1.77a	1.68a
	F	20.91a	19.63a	18.85a	19.59a

<sup>1</sup>Concentrations or mass for a given component with same letters are not significantly different at  $\alpha=0.05$

Differences in Ca, Mg, and Mn among sub-ecoregions did not appear to be related to aboveground production of litter because neither mass of L or F-layers significantly differed among sub-ecoregions. Although it is well documented that increased inputs, cycling, and/or soil availability of Ca and Mg occur with an increased level of hardwoods in a stand (Pritchett, 1987; Binkley and Valentine, 1991), there was no evidence that differences in nutrient concentrations

Table 3. Macronutrient concentrations in pine and hardwood (Hwd) foliage in the L-layer and in the F-layer (F).

		North	East	South	West
		----- mg kg <sup>-1</sup> -----			
<b>Cu</b>	Pine	12a	19a	21a	12a
	Hwd	7a	9a	17a	24a
	F	11ab	10b	12a	11ab
<b>Fe</b>	Pine	136a	170a	177a	169a
	Hwd	273a	237a	255a	498a
	F	6610a	5793a	4313a	4853a
<b>Mn</b>	Pine	1078a	914ab	828b	865b
	Hwd	2121a	1730ab	1593b	1920ab
	F	1803a	947b	1074b	1281b
<b>Na</b>	Pine	133a	179a	187a	137a
	Hwd	104a	69a	132a	196a
	F	723a	776a	725a	766a
<b>Zn</b>	Pine	188a	160a	157a	143a
	Hwd	107a	90a	73a	130a
	F	87a	77a	67a	86a

<sup>1</sup>Concentrations for a given component with same letters are not significantly different at  $\alpha=0.05$

among sub-ecoregions were related to stand composition. Statistical comparisons demonstrated that neither stand hardwood nor pine basal area differed among sub-ecoregions.

Although stand composition and production appear to be similar among the sub-ecoregions, these regions do differ in their climate and geology. Mean annual precipitation is 10-20 cm less in the northern sub-ecoregion than in the other sub-ecoregions (Skiles 1981). Stratigraphy and lithology are two of the most relevant factors used to delineate these sub-ecoregions into separate subsections in the classification system created by Keys et al. (1995). The stratigraphy and lithology of these four subsections are described in the following manner: the northern subsection has (Fourche Mountains) sandstone and shale-clast loamy colluvium, the east (East Central Ouachita Mountains) subsection a chert fragment and quartzite boulder colluvium, the south subsection (Athens Piedmont Plateau) has acid chip clay-loam and bouldery sandy colluvium, and the west subsection (West Central Ouachita Mountains) has acid shale-chip and clay loam colluvium. These differences in geology and climate apparently have influenced the soils within these sub-ecoregions and thus the chemistry of the forest floor. It is interesting to note that although similar species compositions exist within stands, differences in soils attributed to what is assumed to be relatively small differences in climate or geology, have altered the chemistry of the forest floor with sig-



## Variability in Forest Floor Mass and Nutrient Concentration of Mature Pine-Hardwoods in the Ouachita Mountains

nificant enough magnitude to be detected at a moderate sampling intensity.

### Conclusions

Variation in forest floor micro- and macronutrient concentrations in shortleaf pine-hardwood stands was found to be greater among stands occurring in different sub-ecoregions than among slope positions within stands. The lack of any substantial differences in concentrations among slope positions was in part attributed to the methods used to delineate slope position. The criteria utilized for stand and plot selection in this study was not suited for the testing of landform level differences in slope position. Variation in climate and geology appeared to be two of the more important factors contributing to the differences in forest floor nutrient concentrations among subecoregions.

**ACKNOWLEDGMENTS.**—Funds for this research were provided by the USDA Forest Service, Southern Forest Experiment Station.

### Literature Cited

- Baker, J. B.** 1994. An overview of stand-level ecosystem management research on the Ouachita/Ozark National Forests. (Pp. 18-28) *In* Proceedings of the symposium on ecosystem management research in the Ouachita Mountains: pretreatment conditions and preliminary findings; 1993 October 26-27; Hot Springs, AR. Gen. Tech. Rep. SO-112. New Orleans, LA: U.S. Department of Agriculture, Forest Service, Southern Forest Experiment Station.
- Binkley, D. and D. Valentine.** 1991. Fifty-year biogeochemical effects of green ash, white pine, and Norway spruce in a replicated experiment. *For. Ecol. and Man* 40:13-25.
- Clingenpeel, J. A and B.G. Cochran.** 1992. Using physical, chemical, and biological indicators to assess water quality on the Ouachita National Forest utilizing basin area stream survey methods. *Proc. Arkansas Acad. Sci.* 45: 33-35.
- Graney, D. L.** 1992. Site index relationships for shortleaf pine. *In*. Brissette, John C.; Barnet, James P., comp. Proceedings of the shortleaf pine regeneration workshop; 1991 October 29-31; Little Rock, AR. Gen. Tech. Rep. SO-90. New Orleans, LA; U.S.DA, Forest Service, Southern Forest Experiment Station: 142-157.
- Keys, Jr., J., C. Carpenter, S. Hooks, F. Koenig, W.H. McNab, W. Russell, and M.L. Smith.** 1995. Ecological units of the eastern United States—first approximation (map and booklet of map unit tables), Atlanta, GA: U.S. Department of Agriculture, Forest Service.
- Pritchett, W.L.** 1987. Properties and management of forest soils. John Wiley & Sons. New York, 499 pp.
- Shelton, M.G. and E.R. Lawson.** 1994. Forest floor characteristics in mature pine-hardwood stands in the Ouachita Mountains. (Pp. 191-197) *In* Proceedings of the symposium on ecosystem management research in the Ouachita Mountains: pretreatment conditions and preliminary findings; 1993 October 26-27; Hot Springs, AR. Gem Tech Rep. SO-112. New Orleans, LA: U.S. Department of Agriculture, Forest Service, Southern Forest Experiment Station.
- Steel, R. G. D. and J. H. Torrie.** 1980. Second Edition: Principles and procedures of statistics a biometrical approach. McGraw-Hill Book Company. New York, 625 pp.
- Skiles, A.** 1981. Arkansas climate atlas. Little Rock, AR: Arkansas Energy Office; Arkansas Industrial Development Commission. 93 pp.
- University of Arkansas, Soil Test Laboratory.** 1990a. Procedure No. PL-003. Total Plant Tissue Digest-ICAP Analysis. 3 pp.
- University of Arkansas, Soil Test Laboratory.** 1990b. Procedure No. PL-0004. Plant tissue total nitrogen analysis. 3 pp.

# A Method to Correct the Voxel Size in PRESS Localized NMR Spectroscopy

Diana M. Lindquist and Roger M. Hawk<sup>1</sup>

Department of Applied Science  
University of Arkansas at Little Rock  
2801 S. University Avenue, Little Rock, AR 72204

Richard A. Komoroski

Departments of Radiology, Pathology, Psychiatry, and Biochemistry  
University of Arkansas for Medical Sciences  
4301 W. Markham, Little Rock, AR 72205

<sup>1</sup>Corresponding Author

## Abstract

Two techniques commonly used on human magnetic resonance spectroscopy systems to obtain spectra from localized volumes in the brain are point resolved spectroscopy (PRESS) and stimulated echo acquisition mode (STEAM) spectroscopy. PRESS gives a signal twice as large as that obtained with STEAM, but suffers from longer minimum echo times. While STEAM must be used to detect species with short spin-spin relaxation times, PRESS can be used for species with longer relaxation times to give a spectrum with a better signal to noise ratio. Only STEAM was provided for the GE Omega 4.7 T small animal imager used in this laboratory. Therefore, a PRESS pulse program was written for this instrument. With the standard sequence, the sampled voxel is smaller than the prescribed voxel. A larger voxel can be prescribed to increase the sampled volume. A different approach, involving the modification of the gradient strength, has been used in this laboratory. The resulting pulse sequence, with representative profiles, is discussed.

## Introduction

A phosphorus-31 spectrum of muscle introduced *in vivo* nuclear magnetic resonance (NMR) spectroscopy in 1980 (Cady, 1990). An *in vivo* spectrum from rat brain followed in 1983. By 1986, several techniques for obtaining *in vivo* spectra had been developed [Bottomley, 1986]. Two popular techniques for obtaining *in vivo* proton NMR spectra are point resolved spectroscopy (PRESS), which was introduced in 1984 (Bottomley, 1984; Ordidge, et. al., 1985), and a similar technique, stimulated acquisition mode (STEAM) spectroscopy, which was described in a 1987 publication (Frahm, et. al., 1987). Both of these techniques are used with commercial magnetic resonance imagers. They are not as routinely used with small animal imagers.

## Theory

Nuclei precess in a magnetic field at the Larmor frequency, which depends on the magnetic field strength:

$$\omega_0 = \gamma B_0, \quad (1)$$

where  $\omega_0$  is the frequency,  $\gamma$  is the magnetogyric ratio, and  $B_0$  is the magnetic field strength. The magnetogyric ratio for a given nucleus must be determined experimentally.

In the field, a small excess of the nuclei align themselves so that the z components of their magnetic vectors are coaxial with the field. The system has a net magnetic moment,

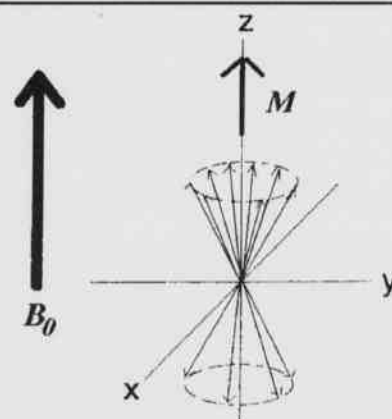


Fig. 1. In an ensemble of spins, a small majority is in the lower energy state. This results in a net magnetic moment,  $M$ , aligned with the main magnetic field,  $B_0$ .

$M$ , which is aligned with the external  $B_0$  field, as shown in Fig. 1.

If an additional field,  $B_1$ , is introduced into the system, a new effective field,  $B_{\text{eff}}$ , is generated. At equilibrium, the net magnetic moment will align itself with  $B_{\text{eff}}$  and the individual nuclei will precess at a frequency given by

$$\omega = -\gamma B_{\text{eff}}, \quad (2)$$

where  $B_{\text{eff}}$  is the magnitude of  $B_{\text{eff}}$ .

## A Method to Correct the Voxel Size in PRESS Localized NMR Spectroscopy

Let  $B_1$  oscillate at the Larmor frequency,  $\omega_0$ , and introduce new coordinate axes which rotate at the same frequency. The new axes are denoted  $x'$ ,  $y'$ , and  $z'$  and are related to the stationary axes as follows: the  $z$  and  $z'$  axes are coincident, while  $x'$  and  $y'$  rotate about  $z$ . In this rotating frame of reference,  $B_1$  appears stationary and the  $B_0$  field disappears (Farrar and Becker, 1971). In the rotating frame, the net magnetic moment rotates about the  $B_1$  field.

For example, let  $B_0$  be oriented along the  $z$ -axis and let  $B_1$  coincide with the  $x$ -axis. In the rotating frame,  $M$  will experience a torque from the  $B_1$  field and rotate onto the negative  $y$  axis, as shown in Fig. 2.

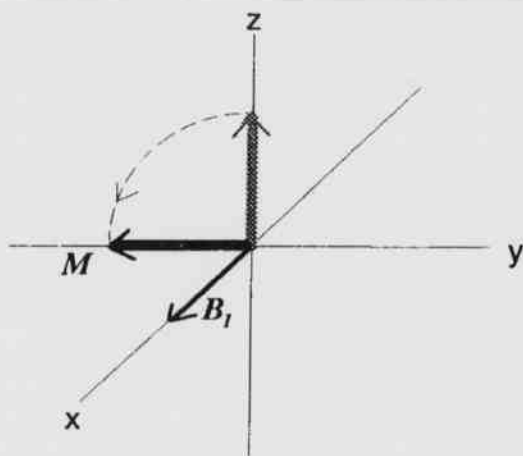


Fig. 2. A  $B_1$  field oscillating at the Larmor frequency is applied along the  $x$ -axis.  $M$  rotates around the  $x$ -axis as long as the  $B_1$  field is applied. Here,  $M$  has rotated  $90^\circ$ .

In the rotating frame, the angle through which the magnetization rotates is given by

$$\theta = \omega t = \gamma B_1 t \quad (3)$$

where  $t$  is the length of time the field is present and  $B_1$  is its magnitude. A pulse of radio frequency (RF) energy at the Larmor frequency provides the  $B_1$  field. If the pulse is long enough to rotate  $M$  by  $90^\circ$ , it is called a  $90^\circ$  pulse. Any desired flip angle can be generated by varying the time for which the RF energy is applied.

After  $M$  has been tipped into the  $xy$  plane and the  $B_1$  field is removed, the spins return to their original alignment along the  $z$  axis. This process is called relaxation. There are two time constants associated with relaxation: the spin-lattice relaxation time,  $T_1$ , and the spin-spin relaxation time,  $T_2$ . The spin-lattice relaxation time is a measure of how long it takes for magnetization along the  $z$  axis to recover; the spin-spin relaxation time is a measure of how long magnetization persists in the  $xy$  plane. In general,  $T_1$  refers to exponential growth and  $T_2$  refers to exponential decay of the rel-

evant magnetization.

A potential problem with NMR is that the pulse excites a range of frequencies. Theory shows that the bandwidth of a simple on-off pulse is approximately equal to the inverse of the pulse length (Farrar and Becker, 1971). If the pulse length is very short, the bandwidth is broad and spins with largely differing Larmor frequencies are excited. If the pulse is very long, spins with only a narrow distribution of Larmor frequencies will be excited. In *in vivo* spectroscopy, the distribution of frequencies is used to achieve spatial localization.

The frequency response of a pulse is approximated by the Fourier transform of its shape in the time domain. The Fourier transform of a rectangular pulse is a sinc function centered at the RF frequency of the pulse. Other frequencies, contained in the middle and side lobes of the response, are also excited. For many purposes, such a broad excitation is undesirable. To excite a plane of spins, for example, the frequency response should be a well-defined rectangular function.

One of many approaches to defining the frequency response is to Fourier transform the desired response. The resulting function is then used to modulate the RF pulse. Since the transform of a rectangular function is a sinc function, a sinc shaped RF pulse gives a more nearly rectangular excitation.

When shaped RF pulses are used, the flip angle is adjusted by changing the power of the pulse. This corresponds to altering the amplitude of the  $B_1$  field. A  $90^\circ$  power level, rather than a  $90^\circ$  pulse width, is defined.

### Localization

Localized NMR experiments must include some means of identifying the position from which the signal originates. Gradients are used in conjunction with the RF pulse to localize the signal.

A gradient is a linearly varying magnetic field that is applied in addition to the  $B_1$  and  $B_0$  fields. Let the strength of this gradient be represented as  $kx$ , for a gradient along the  $x$  axis of magnitude  $k$ . The effective field strength is given by

$$B_{\text{eff}} = B_0 + B_1 + kx \quad (4)$$

Since  $\omega = \gamma B_{\text{eff}}$ , the Larmor frequency now is proportional to  $kx$ . Spins at different  $x$  locations will have different Larmor frequencies. Only those spins with Larmor frequencies in the bandwidth of the RF pulse will be affected. Since frequency now depends on position, bandwidth now corresponds to a range of  $x$  values.

Consider a gradient for which  $k$  is 1 gauss/cm (G/cm), as shown in Fig. 3. Let  $\gamma$  for the nucleus of interest be 4

kHz/G and suppose a 1 ms hard pulse is applied. The bandwidth is then 1/1 ms or 1 kHz. Spins with frequencies  $\pm 1$  kHz from the center frequency will be excited. The gradient corresponds to a frequency change of 4 kHz/cm, so the pulse excites a 0.5 cm length of spins along  $x$ . Since the object to be imaged is three dimensional, a 0.5 cm thick plane of spins perpendicular to the  $x$ -axis has been selected.

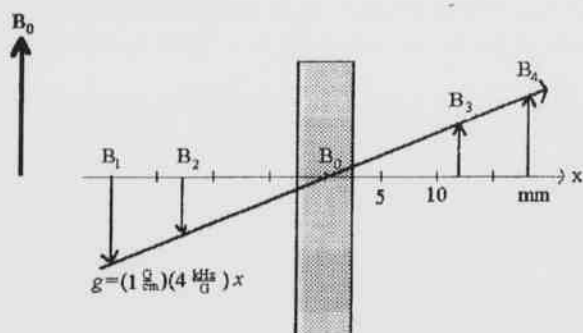


Fig. 3. A 1 ms pulse in the presence of a 1 G/cm  $x$  gradient is applied to a system with a magnetogyric ratio of 4 kHz/G. Since the slope of the gradient is 4 kHz/cm, the +1 kHz of excited frequencies centered about  $\omega_0 = -\gamma B_0$  is mapped into a slab of spins 0.5 cm thick. The shading represents the area of excited spins.

If a gradient subsequently is applied in the  $y$  direction, with a concurrent RF pulse, two planes of spins will be excited. Only along the intersection of those planes will the spins have experienced both pulses. Applying a third gradient along  $z$ , with a simultaneous RF pulse, will selectively excite the intersection of three planes. Figure 4 illustrates this intersection, or voxel.

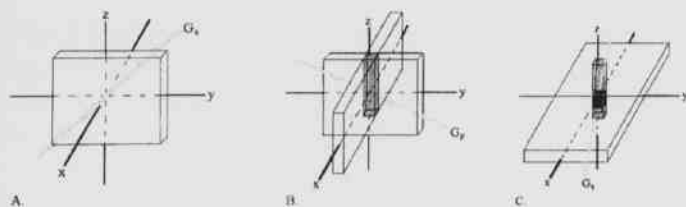


Fig. 4. A. Use of only the  $x$  gradient to select a slab of spins. B. Addition of the  $y$  gradient selects a column of spins, as indicated by the shaded region. C. Addition of the  $z$  gradient selects a box, as shown by the black region in the center. The  $x$  and  $y$  planes have been omitted for clarity. In all cases, the direction of the gradient is indicated by the dotted line.

The signal collected after the final RF pulse can be Fourier transformed to give a spectrum from the excited voxel. However, spins outside the voxel may contribute to the magnetization in the  $xy$  plane at the end of the experiment. Additional gradient pulses are needed to isolate the voxel.

Any sequence that uses multiple RF pulses generates a series of echoes. Hahn showed that, for a sequence of three pulses, a total of five echoes may be generated (Hahn, 1950). Two sequences that utilize these echoes are stimulated echo acquisition mode (STEAM) spectroscopy and point resolved spectroscopy (PRESS).

STEAM uses three  $90^\circ$  pulses to localize the voxel and, therefore, acquires a stimulated echo (Hahn, 1950). PRESS uses a  $90^\circ$  pulse followed by two  $180^\circ$  pulses and acquires a spin echo. The stimulated echo is only half as large as a spin echo acquired from the same region [Hahn, 1950], but the STEAM sequence is preferable for collecting spectra from species with short  $T_2$ 's. PRESS, however, is the preferred sequence if some  $T_2$  relaxation is permissible in the experiment.

### Point Resolved Spectroscopy

Point resolved spectroscopy uses three RF pulses and three gradients to choose a voxel. Figure 5 is a timing diagram for the sequence. The length of time between the first two pulses determines the echo time (TE), which is the interval between the center of the first RF pulse and the start of data acquisition.

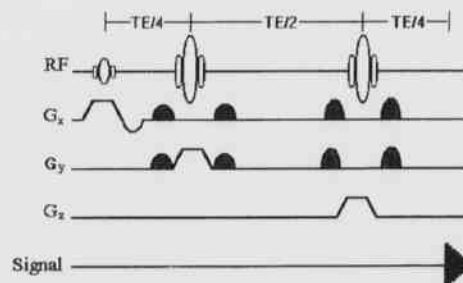


Fig. 5. The PRESS timing diagram.

The first RF pulse is a sinc shaped  $90^\circ$  pulse, which is applied with an  $x$  gradient. This causes the spins within a plane perpendicular to the  $x$  axis to rotate onto the negative  $y$  axis. During  $TE/4$ , the interval between the first two pulses, the spins dephase by an amount  $(\Delta\omega)(TE/4)$ , where  $\Delta\omega$  is the frequency difference between the frequency of the RF



## A Method to Correct the Voxel Size in PRESS Localized NMR Spectroscopy

pulse and the precessional frequency of a given spin. A  $180^\circ$  pulse, with its associated  $y$  gradient, is then applied and flips the spins  $180^\circ$  about the  $y$  axis, without changing the direction in which they rotate. The phase of the spins continues to change, but since the spins that were ahead of  $\omega_0$  are now behind  $\omega_0$ , as seen in Fig. 6, the spins will rephase and form a spin echo  $TE/4$  after the pulse.

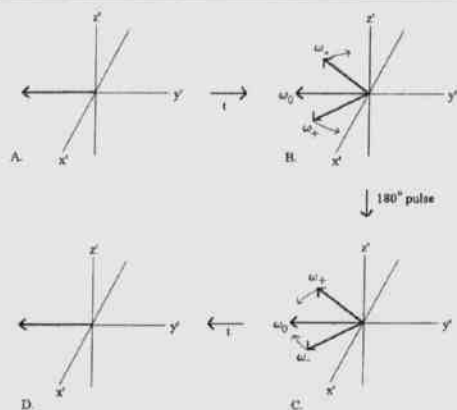


Fig. 6. All diagrams use the rotating frame. A. The spins are in phase in the transverse plane after the  $90^\circ$  pulse. B. The spins have dephased during time  $t$ . The center frequency,  $\omega_0$ , appears stationary, while other spins rotate at the frequencies  $\omega_+$  and  $\omega_-$ . The differing frequencies cause the spins to spread out in the transverse plane. C. After the  $180^\circ$  pulse is applied along the  $y'$  axis, the spins exchange places. D. The spins rephase after a further delay,  $t$ .

Finally, the third  $180^\circ$  pulse is applied  $TE/2$  after the second pulse, which allows the spins to dephase after forming the echo. This pulse again reverses the spins, but only in the voxel, since there is a simultaneous gradient in the  $z$  direction. The rephased spins form a spin echo  $TE/4$  after the last pulse.

Although the entire echo can be sampled, in practice, only the second half of the echo is acquired. The primary reason for this delay is the potential for distortion of the echo due to eddy currents from the switched gradients. The second half of the echo, since it occurs later in time, is less likely to be so distorted. Fourier transformation of the sampled data yields the spectrum.

There are several problems with this sequence, most of which arise from imperfect RF pulses. Ideally, each of the  $180^\circ$  pulses causes the transverse spins in the intersection to rephase while simply inverting longitudinal magnetization. However, some of the longitudinal magnetization actually is rotated into the transverse plane (Jung, 1996). This unwanted

ed magnetization contributes to the final signal and must be eliminated.

"Crusher" gradients are used to destroy the unwanted transverse magnetization. If a gradient is applied after a pulse, it dephases the spins in the transverse plane. Crusher gradients are applied after each  $180^\circ$  pulse to dephase the unwanted  $xy$  magnetization. However, these gradients also destroy the signal from the voxel. To preserve that signal, an equal but opposite gradient must be applied, but only to the spins in the voxel.

Let C2 be the gradient immediately after the  $180^\circ$  pulse and let its slope be  $k$ . In the rotating frame, this gradient causes spins in the transverse plane to dephase by

$$\Delta\theta = 2\pi\gamma kxt, \quad (5)$$

where  $x$  is the coordinate of the spin,  $t$  is the duration of C2, and  $\Delta\theta$  is the phase difference with respect to  $x = 0$ .

If a gradient identical to C2 is applied immediately prior to the  $180^\circ$  pulse, the transverse magnetization will dephase by  $\Delta\theta$ . The spins in the voxel change places after the  $180^\circ$  pulse and will rephase when C2 is applied, while any new transverse magnetization is dephased. This is identical to Fig. 6, except that now a gradient is used to dephase and rephase the spins, rather than a delay time,  $t$ . Therefore, to preserve the spin echo, the crusher gradients must be applied symmetrically around the  $180^\circ$  pulse.

The equations which describe the effects of an RF pulse are nonlinear and, for large tip angles, the simple inverse relationship between bandwidth and pulse duration is no longer applicable (Ernst, et. al., 1987; Yan, et. al., 1987; Yan and Gore, 1987a; Yan and Gore, 1987b). The nonlinearity of the response causes a smaller frequency range to be excited for the  $180^\circ$  pulse than for the  $90^\circ$  pulse (Yan, et. al., 1987; Yan and Gore, 1987a; Yan and Gore, 1987b), which results in narrower planes of excited spins. This is shown in Fig. 7. The profiles were obtained using the standard PRESS sequence and correspond to the width of the plane selected by each pulse.



Fig. 7. Profiles obtained using the unmodified PRESS sequence. A. Profile in the  $x$  direction using a  $90^\circ$  pulse. B. Profile in the  $y$  direction from a  $180^\circ$  pulse. C. Profile in the  $z$  direction.

There are three ways to correct the voxel size: prescribe a larger voxel than is actually desired, increase the bandwidth of the 180° pulses, or reduce the gradient strengths which are applied with those pulses (Jung, 1996; Moonen, et. al., 1989). While prescribing a larger voxel is the simplest solution, it requires the operator to make an accurate estimate of the necessary increase in size. Increasing the bandwidth is undesirable because it makes programming and optimizing the sequence timing difficult. For example, increasing the pulse length or number of lobes in the 180° sinc pulse would increase the bandwidth, but then the power for the pulse would not be related easily to the power for the 90° pulse. By keeping the two pulse shapes identical, the power level for the 180° pulse is just twice that of the 90° pulse. The third alternative is the best solution because the reduction in gradient strength is constant for a given system.

For our system, a GE Omega CSI 4.7 T instrument controlled by a Sun 3/160 workstation, the gradients applied with the 180° pulses need to be reduced by 30% to achieve the correct voxel size at half maximum. This reduction is achieved by multiplying the calculated gradient strength by a scaling factor of 0.7.

The apparent gradient strength, using the Fourier transform approximation, is given by

$$G_{app} = \text{sinc}l / (\text{sinc}l \cdot st) \quad (6)$$

where  $G_{app}$  is the apparent gradient strength,  $\text{sinc}l$  is the number of lobes in the sinc pulse,  $\text{sinc}l$  is the length of time for which the pulse is applied, and  $st$  is the desired slice thickness. The actual gradient strength used is given by

$$G_{act} = sf \cdot G_{app} \quad (7)$$

where  $sf$  is the scaling factor.

Profiles obtained from the PRESS sequence using the default scaling factor of 0.7 are shown in Fig. 8. Empirical measurements with this system have shown that a scaling factor of 0.7 gives the desired voxel size. A scaling factor of 0.775 was required for a similar instrument (Moonen et. al., 1989). Since the scaling factor is constant, it can be evaluated once and programmed into the sequence. Such a default correction allows the operator to prescribe a voxel without having yet another parameter to adjust.

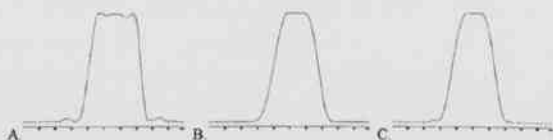


Fig. 8. Profiles from the modified PRESS sequence. A. Profile from the 90° pulse. B. Profile from the first 180° pulse. C. Profile from the second 180° pulse.

The profiles of the 180° planes are not perfectly rectangular. This can be improved by adjusting either the shape of the gradient pulse (Yan and Gore, 1987a), by using multiple RF pulses (Yan and Gore, 1987b), or by using special shaped pulses (Shinnar et. al., 1989a; Shinnar et. al. 1989b). These solutions require either an increase in the complexity of the program or an increase in the duration of the pulse sequence. For some purposes, such increases may be necessary. When they are not, a scaling factor provides a simple means of improving the voxel size.

## Conclusion

The PRESS pulse sequence is a good alternative to STEAM for localized *in vivo* NMR spectroscopy. However, it uses 180° pulses, which, due to the nonlinearity of the system, cause unwanted magnetization to contribute to the signal from a voxel that is too small. Careful optimization of the crusher gradients and the slice selection gradients used with these pulses is required. The improper adjustment of the crusher gradients will result in the spin echo being contaminated with signal from outside the voxel. If the slice selection gradients are not adjusted, the sampled voxel will be smaller than desired. Although several methods have been proposed to adjust the voxel size, the simplest method is to multiply the calculated gradient strength by a scaling factor. This scaling factor is constant for a given system, so it can be determined once and incorporated into the pulse program. The operator has one less parameter to adjust, and the program is still easy to implement. The scaling factor is a simple way to make the pulse program both user friendly and accurate.

## Literature Cited

- Bottomley, P. A. 1984. US patent 4,480,228.
- Bottomley, P. A. 1986. A practical guide to getting NMR spectra *in vivo*. Pp. 81-95, *In Medical Magnetic Resonance Imaging and Spectroscopy: A Primer*, (F. F. Budinger and A. R. Margulis, eds.) Society of Magnetic Resonance in Medicine. 272 pp.
- Cady, E. B. 1990. *Clinical Magnetic Resonance Spectroscopy*. Plenum Press, New York, 278 pp.
- Ernst, R. R., G. Bodenhausen, and A. Wokaun. 1987. *Principles of Nuclear Magnetic Resonance in One and Two Dimensions*. Oxford Science Publications, Oxford, 610 pp.
- Farrar, T. C. and E. D. Becker. 1971. *Pulse and Fourier Transform NMR*. Academic Press, New York, 115 pp.
- Frahm, J., K. D. Merboldt, and W. Hänicke. 1987. *Localized proton spectroscopy using stimulated echoes*.

A Method to Correct the Voxel Size in PRESS Localized NMR Spectroscopy

---

- J. Magn. Reson. 72:502-508.
- Hahn, E. L.** 1950. Spin Echoes. *Physical Review*, 80:580-594.
- Jung, W. I.** 1996. Localized Double Spin Echo Proton Spectroscopy Part I: Basic Concepts. *Concepts in Mag. Res.* 8:1-15.
- Moonen, C. T. W., M. von Kienlin, P. C. M. van Zijl, J. Cohen, J. Gillen, P. Daly, and G. Wolf.** 1989. Comparison of Single-shot Localization Methods (STEAM and PRESS) for *In Vivo* Proton NMR Spectroscopy. *NMR in Biomed.* 2:201-208.
- Ordidge, R. J., M.R. Bendall, R.E. Gordon, and A. Connelly.** 1985. Volume selection for *in vivo* biological spectroscopy. Pp. 387-397, *In Magnetic Resonance in Biology and Medicine* (G. Govil, C. Khetrpal, and A. Saran, eds.) Tata McGraw-Hill Publishing Company, Ltd., New Delhi, 479 pp.
- Shinnar, M., L. Bolinger, and J. S. Leigh.** 1989a. The synthesis of soft pulses with a specified frequency response. *Magn. Reson. Med.* 12:88-92.
- Shinnar, M., S. Eleff, H. Subramanian, and J. S. Leigh.** 1989b. The synthesis of pulse sequences yielding arbitrary magnetization vectors. *Magn. Reson. Med.* 12:74-80.
- Yan, H. and J. C. Gore.** 1987a. A novel analysis of selective excitation and phase reversal. *J. Mag. Reson.* 73:448-458.
- Yan, H. and J. C. Gore.** 1987b. Improved selective 180° radiofrequency pulses for magnetization inversion and phase reversal. *J. Mag. Reson.* 71:116-131.
- Yan, H., B. Chen, and J. C. Gore.** 1987. Approximate solutions of the Bloch equations for selective excitation. *J. Mag. Reson.* 75:83-95.

# Prediction of Potential Antimigraine Activity Using Artificial Neural Networks

Qing Luo, Jerry A. Darsey and Cesar M. Compadre  
Department of Chemistry  
University of Arkansas at Little Rock  
Little Rock, AR 72204

Sanjay K. Mitra  
Department of Chemistry  
University of Arkansas at Little Rock  
Little Rock, AR 72204

Department of Biopharmaceutical Science  
University of Arkansas for Medical Sciences  
Little Rock, AR 72205

## Abstract

More than 10 million Americans, three quarters of them women, suffer some degree of recurrent migraine headaches. Feverfew (*Tanacetum parthenium* (L.) Schultz-Bip.) is a member of the Asteraceae family that is native to Europe. This plant is a perennial flowering aromatic plant common in gardens. It has been widely used as a self-medication of arthritis, fever, and migraine headaches for over 2000 years. Sesquiterpene lactones (SL) are the components responsible for the antimigraine activity of feverfew. In this research, the relationship between SL structural information and their biological activity was studied by using Gaussian 92 program in conjunction with artificial neural networks (ANNs). The molecular orbital parameters of SL were obtained by using Gaussian 92 program. A set of 39 SL molecules was divided into two groups, a training set containing 33 molecules and a testing set containing six molecules. An ANN was trained and tested by using training sets and testing sets on SL's antimigraine activities. The results showed that ANNs successfully predicted the antimigraine activities of SL based on their different structural information.

## Introduction

Migraine headaches are highly prevalent disorders, they can be physically and psychologically disabling. More than ten million Americans, three quarters of them women, suffer some degree of recurrent migraine headaches. Migraine can affect any age group but the peak years are ages between 25 and 55. The annual cost of medical care and lost productivity because of migraines in the United States has been estimated to range from \$1.2 billion to \$17.2 billion (Lipton et al., 1993). It really has become an economic burden on society. Furthermore, reports of migraine in the United States have increased dramatically since 1980, for example, migraines prevalence increased 60% from 1981 to 1989 (Lipton et al., 1997).

Serotonin (5-hydroxytryptamine or 5-HT) is considered to be one of the most important neurotransmitters associated with migraine headaches since recent studies showed that the distribution of 5-HT in the blood of migraine patients differs from that in control subjects. Release of 5-HT from blood platelets can constrict blood vessels and contribute to migraine pain. The antimigraine activity of SL was expressed by the inhibition of serotonin released from platelets by the SL (Marles et al., 1995).

Biological activity of any compound is a direct consequence of its molecular structure, investigations of the

relationship between chemical structure and the activity of compound are helpful in understanding the activity of interest and in predicting the activity of new compounds based on knowledge of the chemical structure alone.

This paper discusses one approach which employs self-consistent field-molecular orbital (SCF-MO) quantum mechanical calculations (Clark, 1985) in conjunction with artificial neural networks on prediction of antimigraine activity of SL. The structural information of SL were obtained by using Gaussian 92 program and ANN was trained and tested on the antimigraine activities of 39 SL.

## Materials and Methods

Computational studies were performed using Silicon Graphic's R4400 or R4600 computers. There are three main steps used in this research. First, SL structures were obtained directly from Cambridge Structural Database (Cambridge Crystallographic Data Centre, Cambridge, UK) or built by modification of related structures available in this database using some tools in SYBYL 6.2 (Tripos associates, St. Louis, MO, USA). The geometry of lowest energies of each molecule was obtained for the further investigation.

Second, quantum mechanical calculations using the Gaussian 92 program were run on each SL structure to



## Prediction of Potential Antimigraine Activity Using Artificial Neural Networks

obtain their structural information, such as eigenenergy and dipole moment. The input for the calculations was an internal coordinate matrix (Z-matrix) of the SL structure with lowest energy. The basis set used was a STO-3G\* and POP=REGULAR was used as a keyword to do the regular population analysis. The eigenenergies of the lowest fifteen unoccupied molecular orbitals, the highest fifteen occupied molecular orbitals and the dipole moment of each molecule were chosen from the output file of Gaussian 92.

Finally, ANNs were employed to make the necessary correlation between structural information and the antimigraine activity of SL. The antimigraine activity data of SL were measured as their ability to inhibit the release of serotonin ( $IC_{50}$ ) and previously reported by Marles and co-workers (1995).  $IC_{50}$  is the micromolar concentration of SL that will inhibit the release of serotonin by 50%.

ANNs are computer models that were first developed based on the neural structure of the brain. The brain basically learns from experience. In particular, the most basic element of the human brain is a specific type of cell known as neurons. The power of the human mind comes from the large numbers of these basic components and the multiple connections between them. ANNs are massively parallel computing systems made up of a number of simple, highly interconnected processing elements which process information by determining the value of an output signal based on the values of several input signals. Figure 1 shows a three layer fully connected ANN.

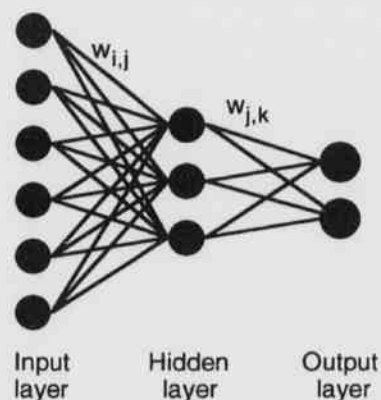


Fig. 1. Architecture of a three layer Artificial Neural Network.

ANN used in this research is error back propagated supervised neural network. It was first developed by McClelland and Rumelhart (McClelland and Rumelhart,

1986). It has been successfully used in our previous studies (Darsey, et.al, 1993; Soman, et al, 1995). As shown in Fig. 1, it has three layers inside of the network: input layer, hidden layer and output layer. Each layer usually includes several processing elements (or neurons, nodes, etc) which are the basic element of neural network. The nodes of the input layer are responsible for the distribution of the input to the next layer of nodes. One hidden layer is placed between the input and output layers.

In this case, 31 nodes which included 30 eigenenergies and 1 dipole moment, were placed in input layer, 12 nodes were used in hidden layer and only 1 node was used in output layer which was antimigraine activity of SL. All these nodes were interconnected through unidirectional connection (weights). Weights are adaptive coefficients that are changed when the network learns. Randomly set weights are used at the beginning and then adjusted by the network so that the next cycle will produce a closer match between the desired and the actual output (Haykin, 1994).

The operations in a processing element started with the computation of the weighted sum of all of the inputs. This weighted sum input, then, was transformed to a working output through a transfer function. The most used transfer function is a sigmoid function. It is used to map the weighted sum of the input values to a reasonable value, before passing the signal into the nodes in next layer. The reasonable values accepted by neural networks are between 0 and 1.

The network learns when it is trained based on a data driven system. Backpropagation network processes the inputs and compares the resulting outputs to the actual outputs. Outputs errors are propagated back through the system, causing the system to readjust the weights. This process runs over and over until continually tweaking the weights.

Once, the network is "taught" how to respond to a set of specific examples, these weights are stored. The network is tested for the accuracy of its predictions of biological activities of SL not included in the training set, using these weight. The dataset which included eigenenergies and dipole moments of 39 SL was divided into two group, one group (training set), which included 33 SL, was used for training the network and another group (testing set), which included six SL, for testing the network prediction. Then, an ANN was trained by using training set to a satisfactory error limit 0.001 and tested by using testing set. This training and testing process were repeated by using different set of training and testing set until all the SL wer predicted once.

## Results and Discussion

The basis set used in Gaussian 92 program is STO-3G\*, the selection of this basis set is a compromise between qual-

Table 1.

Compound Name	Biological Activity <sup>1</sup>		
	Observed Data	Predicted Data	Error %
Ursinoliide A	5.75	5.68	-1.22
Cinereenin Acetate	5.69	5.71	0.35
Parthenolide	5.52	5.61	1.63
Cinereenin	5.45	5.83	6.97
Cnicin	5.45	5.42	-4.95
Helenalin	5.37	5.19	-3.35
Melampodin A	5.29	5.23	-1.13
Ursinoliide B	5.28	5.32	0.76
Alatolide	5.26	5.22	-0.76
Stizolicin	5.24	5.67	8.21
Centaurepensis	5.22	5.23	0.19
Repin,15-deoxy	5.20	5.23	0.58
Arbusculin B,1 β-hydroxy-8β-epoxyangeloyloxy	5.18	5.45	5.21
Santamarin,8β-O-epoxyangelate	5.15	5.14	-0.19
Enhydrin	5.06	5.02	-0.79
Confertiflorin	5.05	5.39	6.73
Repin	5.03	4.91	-2.39
Reynosin,8β-0-2,3-dihydroxy-2-methylbutyrate	5.02	5.01	-0.20
Reynosin,8β-O-epoxyangelate	4.99	5.04	1.00
Salonitenolide	4.99	5.44	9.02
Linifolin A	4.94	4.97	0.61
Santamarin,3,4-cis-α-epoxy-8β-epoxyangeloyloxy	4.75	4.72	-0.63
Glaucolide A	4.68	4.64	-0.85
Grossheinin	4.65	4.57	-1.72
Santamarin,8β-0-(2-hydroxy-ethyl) acrylate	4.75	4.60	0.66
Tatridin B	4.57	4.56	-0.22
Parthenolide, 1,10-dihydro-	4.39	4.36	-0.68
Psilostachyin A	4.36	4.29	-1.61
Asperilin	4.24	4.27	0.71
Aromaticin,6α-hydroxy-2,3-dihydro	4.22	4.16	-1.42
Geigerinin	4.14	4.13	-0.24
Santamarin	4.07	4.09	0.49
Xerantholide	3.99	4.00	0.25
Parthenin	3.89	3.86	-0.77
Vachanic acid,methyl ester	3.70	3.71	0.27
Coronopilin	3.60	3.62	0.56
Burrodin	3.60	3.57	-0.83
Reynosin	3.57	3.54	-0.84
Schkuhriolide	3.56	3.53	-0.84

<sup>1</sup>Biological activity is the Log (1/IC<sub>50</sub>) where IC<sub>50</sub> is the micromolar concentration of SL that will inhibit the release of serotonin by 50%. Values were taken from Marles et al. (1995).

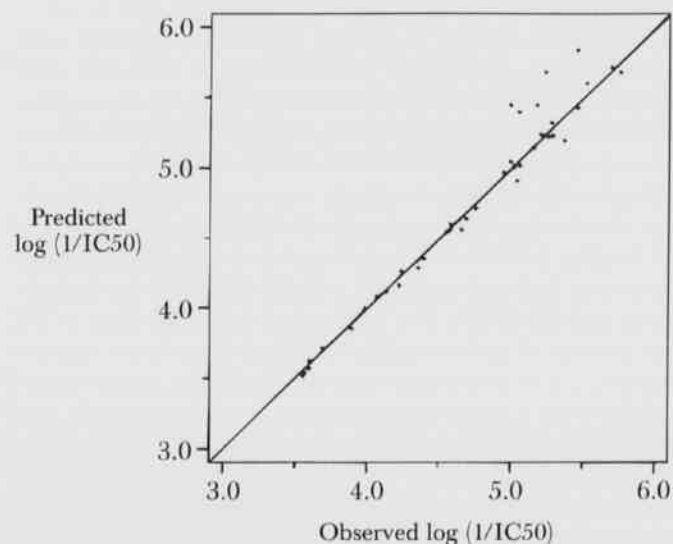


Fig. 2. Correlation between the actual values and the predicted values of biological activities of SL by using ANN.

ity of the results and availability of computer resources. More detailed basis sets such as 6-31G, that could potentially provide higher quality results. However, it produced files larger than the two-gigabyte limit that the computer operating system (IRIX 5.3) could handle.

ANNs analysis of the antimigraine activity of SL was performed as indicated in the methods section, with a training set of 33 SL and a testing set of 6 SL. Several runs were conducted in this manner. The results of this analysis are presented in Table 1, and a plot of predicted versus observed activity is presented in Fig. 2. It can be observed that the percent error for prediction of antimigraine activity of SL ranged from a minimum of -0.19 to a maximum of -9.02. These errors are very low and most of them are probably smaller than experimental error. Figure 2 also showed that ANNs did very well in correlating the structural information and their antimigraine activity of SL since most of the data are in the straight line in this plot.

## Conclusions

In this research, we have demonstrated the use of ANNs in mapping quantum mechanical parameters to antimigraine activities of SL. ANNs were found to be very successful in correlating the SL's structure with their antimigraine activity, although they provided very limited information on the particular requirements for maximum activity.

## Prediction of Potential Antimigraine Activity Using Artificial Neural Networks

---

Additional studies on the structure-toxicity relationship studies of the SL using ANNs should be very helpful in identifying or designing SL with high activity and low toxic potential. Also, this method might be applied to map quantum mechanical parameters to other chemical, physical and biological properties of different groups of molecules.

### Literature Cited

- Clark, T.** 1985. A handbook of computational chemistry: A practical guide to chemical structure and energy calculations. New York. 233-326 pp.
- Darsey, J. A., A. G. Soman and D. W. Noid.** 1993. *Macromol. Chem.: Theory and Simulation* 2:711.
- Haykin, S.** 1994. *Neural Networks: A comprehensive foundation.* Macmillan College Publishing Company. New York. 138-236 pp.
- Lipton, R.B., Stewart and F. Walter.** 1993. Migraine in the United States: Epidemiology and health care use. *Neurology* 43: (suppl. 3):6-10.
- Lipton, R.B., Stewart and F. Walter.** 1997. Prevalence and impact of migraine. *Neurologic Clinics* 15:1-13.
- Marles, R.J., L. Pazos-Sanou, C.M. Compadre, J. M. Pezzuto, B. Drozds and J.T. Arnason.** 1995. Sesquiterpene Lactones Revisited: Recent Developments in the Assessment of Biological Activities and Structure Relationships. *Recent Adv. Phytochem.* 29:333-356.
- McClelland, T.L. and D.E. Rumelhart.** 1986. *Parallel distributed processing.* Cambridge: The MIT Press.
- Soman, A.G., J.A. Darsey, D.W. Noid and B. G. Sumpter.** 1995. Correlating physical properties of chemical compounds using neural networks. *Int. J. Chem. Biotech.* 13:43.